Schwann-cell cylinders grown inside hyaluronic-acid tubular scaffolds with gradient porosity

Vilariño-Feltrer G[1#], Martínez-Ramos C[1#], Monleón-de-la-Fuente A[1], Vallés-Lluch A[1], Moratal D[1], Barcia Albacar JA[2], Monleón Pradas M[1*]

[1] *Center for Biomaterials and Tissue Engineering, Universitat Politècnica de València, Cno. de Vera s/n, 46022, Valencia, Spain*

[2] *Servicio de Neurocirugía, Hospital Clínico San Carlos, Instituto de Investigación Sanitaria San Carlos (IdISSC), C/ Profesor Martín Lagos, S/N. Madrid, 28040, Spain*

** Corresponding author. Tel.: +34963877277; fax: +34963877276. E-mail: mmonleon@ter.upv.es*

 # Guillermo Vilariño-Feltrer and Cristina Martínez-Ramos contributed equally to this work

Abstract

Cell transplantation therapies in the nervous system are frequently hampered by glial scarring and cell drain from the damaged site, among others. To improve this situation, new biomaterials may be of help. Here, novel single-channel tubular conduits based on hyaluronic acid (HA) with and without poly-L-lactide acid fibers in their lumen were fabricated. Rat Schwann cells were seeded within the conduits and cultured for 10 days. The conduits possessed a three-layered porous structure that impeded the leakage of the cells seeded in their interior and made them impervious to cell invasion from the exterior, while allowing free transport of nutrients and other molecules needed for cell survival. The channel's surface acted as a template for the formation of a cylindrical sheath-like tapestry of Schwann cells continuously spanning the whole length of the lumen. Schwann–cell tubes having a diameter of around 0.5 mm and variable lengths can thus be generated. This structure is not found in nature and represents a truly engineered tissue, the outcome of the specific cell-material interactions. The conduits might be useful to sustain and protect cells for transplantation, and the biohybrids here described, together with neuronal precursors, might be of help in building bridges across significant distances in the central and peripheral nervous system.

Keywords: nervous system regeneration, hyaluronic acid, Schwann cell, protective barrier, cell sheet.

1. Introduction

Ideas for neural cell therapies have flourished since it was discovered that tissue regeneration was viable [1] even in the central nervous system (CNS) [2,3]. However, the regeneration in CNS tracts has not proved to be satisfactory due to the meager axonal growth rate of adult neurons [4,5] and neurite retraction after a short time if no synaptic connection has been reached [6]. In addition, astrocyte activation after trauma leads to a glial scar which, though advantageous in preventing the lesion from spreading, is detrimental for the reconnection of neural populations [7].

Proposals to overcome these difficulties involve the use of systems composed of biocompatible structures acting as a provisory extracellular matrix, exogenous or endogenous healthy cells transplanted within scaffolds, and different cytokines or molecular cues to provide a regenerative guide [8]. A number of studies aiming at the repair of nerve or brain tissue have been conducted with promising results, especially those which used cylindrical or tubular structures to mimic nervous tracts [9-11]. These anisotropic structures provide physical guidance for cell migration and axonal penetration and elongation and they permit the investigation of the effects of guidance stimuli to achieve efficient functional regeneration.

Schwann cells (SCs) are the main supportive cells of neurons in the peripheral nervous system (PNS), and play an important role in neurodegeneration and protection: they have an immunomodulatory effect and they wrap axons creating the myelin sheath around them [12,13]. Furthermore, they constitute a source of multiple growth factors which promote axon regeneration and angiogenesis [14,15]. SCs have been extensively employed in *in vitro* cultures [16,17] and *in vivo* models [18,19] as candidates for restoring defects in nerve bundles. Although they are cells of the PNS, Schwann cells

are able to regenerate and myelinate axons also in the CNS when transplanted [20-22]; for these reasons, SCs have been proposed as cells for transplantation in therapies for spinal cord injury and other CNS disorders [23-28].

However, *in vivo* experiments with glia, neuronal precursors and stem cells [29,30] show a significant loss of transplanted cells at the site of grafting, leading to a poor restoration of functional properties [31]. In order to face this problem, porous scaffolds with tailored properties and structure can be used to provide to the cells a more friendly environment and to prevent them from spreading out of the lesion site [18,19,32].

Different types of hyaluronic acid (HA)-based scaffolds have been implanted into CNS lesions to evaluate their biocompatibility and potential for inducing neural regeneration [32-35]. HA is a glycosaminoglycan present naturally in the extracellular matrix of several tissues in the human body. As a biomaterial, it is biodegradable, biocompatible and resorbable. It is composed of hydrophilic polymeric chains and has numerous advantages compared with other hydrogels, since it can be easily processed, delivered in a minimally invasive way, and has mechanical properties similar to tissues [36,37]. In addition, its degradation rate and the diffusion of active molecules through it can be modulated by selecting a specific range of molecular weights, or by using different crosslinking agents and fabrication procedures. Furthermore, HA induces a low inflammatory response and may contribute to neovascularization through its low-molecular weight oligomers [32,38,39]; in addition, it can be functionalized variously to improve cell adhesion, proliferation, migration and differentiation [40,41]. For all these reasons, HA seems a promising material for nerve and brain tissue repair [32,39-42].

The stabilization of the HA hydrogel through crosslinking [43,44] is mandatory if one wishes to obtain structures that are insoluble and capable of retaining their shape. Here

we employ divynil sulfone (DVS) as a cross-linking agent. DVS is known to be toxic because of the reactivity of its vinyl groups [45,46], so its use implies a risk of toxicity if remnants of this molecule are not completely washed from the material. However, once reacted with the OH groups of the HA molecule these double bonds disappear, and, if non-reacted molecules are thoroughly removed, the resulting HA-DVS networks are devoid of inflammatory, pyrogenic or cytotoxic effects [47-50]. HA-based materials employed in clinic for several uses in humans contain HA-DVS networks and count with FDA approval [51,52].

In the present work, a concept is developed which might find application in the regeneration of neural tracts in the CNS and of nerves in the PNS. A HA conduit with a cylindrical inner channel and aligned poly-L-lactic acid (PLLA) microfibers located in its lumen has been produced and characterized, and tested for cultures of Schwann cells. The concept rests on the hypothesis that the regeneration of neural tracts will require a niche of cells supportive for axon growth (such as Schwann cells and maybe other neuroglia) and a structured, directional material substrate, onto which neurons may project their axons. In our concept this directional substrate is provided by the PLLA microfibers, while the HA conduit, thanks to the peculiar pore morphology of its walls, should be able to isolate and protect the transplanted supportive cells seeded in its interior from the external hostile microenvironment, permitting oxygen and nutrients exchange and removal of waste products. The Schwann cells in the interior of the conduit, besides being a pump for neurotrophic and angiogenic factors, should act as natural scaffolding for axon outgrowth, and the microfibers should guide axonal growth. Our study represents, thus, a first step in this wider concept; here solely the interaction of Schwann cells with the materials of the conduit has been investigated and characterized.

2. Materials and methods

2.1. Materials preparation

A polytetrafluoroethylene (PTFE) thin block with 1.5 mm-wide grooves of square section was used as a mold for the conduits (sketch in Figure 1A). In each groove, a single poly-ε-caprolactone (PCL; PolySciences) fiber of 400-450 μm diameter was located using PTFE washers having external diameters of 1.5 mm every 3 cm of fiber in order to keep it centered. These fibers acted as a template for the lumen of the conduits. Solutions of HA (1.5-1.8 MDa, from Streptococcus equi; Sigma-Aldrich) 1, 3 and 5% wt/wt in sodium hydroxide 0.2 M (NaOH; Scharlab) were prepared by gently stirring for 24 h. Conduits made with such solutions are named onwards HA1, HA3 and HA5, respectively. Divinyl sulfone (DVS; Sigma-Aldrich) was then added as a crosslinker (via a Michael 1,4-addition reaction) in a 9:10 DVS:HA monomeric units molar ratio. Following its addition, the solutions were stirred for 10 s more and injected in the mold grooves.

After 10 min the mold was set in a closed Petri dish to avoid evaporation and chilled to -20ºC for a minimum of 5 h. After fully frozen, the solution in the mold was lyophilized (Lyoquest-85, Telstar) for 24 h at 20 Pa and -80ºC to generate HA microporous matrices due to the sublimation of water crystals. Next, the channel-generating PCL fibers were carefully removed, resulting in the final conduits. One of the exterior surfaces of the conduit, thus, remains in contact with air during the fabrication process. This upper side of the conduit will be referred to as its *top face*. Finally, the conduits were hydrated in distilled water for 2 h, cut 6 mm length, and stored at 4ºC in sterile water until use (up to 4 weeks).

HA porous films (hereinafter HAf) were also prepared by injecting the 5% wt HA solution with DVS in the same proportion as above in a glass *Petri* dish and drying

them for 24 h under a ventilation hood at RT, in order to compare them with the conduits and study the effect of the 3D architecture.

In some of the HA5 conduits thus prepared 20 PLLA fibers of 30 μm diameter (Natureworks 6251D, Ingeo) were located inside their channel, as a loose bundle of individual fibers; the conduits-with-fibers thus prepared are henceforth referred to as HA5-PLLA conduits. Also, PLLA films (hereinafter PLLAf) were solvent-cast from PLLA pellets (PURASORB PL 18 with inherent viscosity 1.8dl/g, Corbion Purac) at 10% w/v in chloroform in a *Petri* dish and air-dried for 24 h at RT. The HAf and PLLAf membranes obtained were die-cut into 7 mm-diameter discs, to obtain a seeding area in the planar substrates comparable to glass coverslips (same size), used as positive controls in cell culture experiments.

2.2. Morphological analysis

The conduits' structure and microporosity was observed, after coating with gold the lyophilized samples, in a JSM 6300 scanning electron microscope (SEM; JEOL) at 10 kV. Some HA5 and HA5-PLLA scaffolds were cut longitudinally and transversely to examine their inner structure and the lumen surface.

2.3. Swelling assay and determination of the conduits' dimensions

The water uptake of HA1, HA3 and HA5 was assessed by weighing them in their dry state, m_0, and at different times, m_t, after keeping them at 37ºC in a closed chamber with controlled relative humidity of 100%. Four replicates per sample were measured. The water content, WC, was defined as the ratio of the mass of water absorbed at each time and the mass of the dry HA, $\frac{m_t - m_0}{m_0}$. Immersion experiments in distilled water and in physiological solution (DBPS; Sigma-Aldrich) were performed similarly by immersing

four samples of HA3 and HA5 conduits for up to 4 h, but the swelling rate was so fast that only the equilibrium water content EWC (i.e. the WC after 10h equilibration) was determined. In these experiments, the liquid water contained in the conduit's channel was removed before weighing. Thus the WC values in these experiments comprise both the water retained in the conduits' micropores and the water taken up by the HA matrix chains, while in the controlled-atmosphere sorption experiments only water taken up by the HA chains is recorded.

The characteristic dimensions of transverse sections of HA3 and HA5 conduits, both in dry and wet states (more than 10h swelling immersed), were determined from photographs taken with a camera and a diffuse-light high-contrast background. From these photographs, and with the ImageJ processing software (NIH Research Services Branch, USA), the length of the side of the cross-section, l_s, and the lumen area, A_0, were determined. The lumen diameter was calculated from the area, $A_0 = \frac{\pi \cdot d^2}{4}$, where d is the diameter, assuming circularity (which was of 0.9 or higher as checked for 8 replicates). The conduit lengths before and after swelling were measured with a micrometer. Data from the conduits' main dimensions were represented as the relative dimensional variation (i.e. dimension in swollen state / dimension in dry state). No results were gathered for the HA1 conduits in these experiments (EWC in immersion and dimensional variations due to swelling) because their extreme softness and high EWC impeded safe handling and no reproducible data could be obtained.

For the calculation of diffusion coefficients an external equivalent diameter, d_{eq}, of the conduits was needed, which was determined for rectangular section cylinders in accordance with the ANSI/ASHRAE 130 standard:

$$d_{eq} = 2b\left(\frac{\pi^{2n}\left(1+\frac{a}{b}\right)^{1+n}}{\left(\frac{a}{b}\right)^{3}}\right)^{1/n-5} \quad \textbf{(1)}$$

In this case, $n \approx 0$, and both a and b were l_s.

The approximate solution at short times for the one-dimensional Fick diffusion equation for a thin slab of thickness e is [53],

$$\frac{M_t}{M_\infty} = \frac{m_t - m_0}{m_\infty - m_0} = 4 \cdot \sqrt{\frac{Dt}{\pi e^2}} \quad \textbf{(2)}$$

where M_t/M_∞ is the fractional water uptake and D is the diffusion coefficient. Assuming that this equation is valid for the conduits and that they have radial symmetry, the diffusion coefficients of water through the hydrogels were calculated. The wall thickness was taken in each case as $e = (d_{eq}-d)/2$ for the three HA concentrations (HA1, HA3 and HA5) with the data collected in the swelling assay.

2.4. Cell cultures

Primary rat Schwann cells (SCs, Innoprot) were employed for cell cultures in the materials. SCs were grown in flasks to confluence at 37ºC, 5% CO_2, in a serum positive culture medium with growth factors (Schwann cells medium kit, Innoprot). Cell culture experiments were performed on one lateral face (excluding the top face) of HA scaffolds (HA5), on HA scaffolds with their lumen empty or filled with 20 PLLA fibers (HA5-PLLA), on HA films (HAf), on PLLA films (PLLAf), on single-PLLA fiber bundles of 20 fibres, and on coverslips as controls. All materials were sanitized and preconditioned for cell culture by two successive rinses with ethanol 70º (Scharlab) for 1 h each in a laminar flow cabinet, and then rinsed with ethanol 50º and 30º for 10 minutes each, followed by a final rinse thoroughly with deionized water. They were preconditioned overnight in culture medium at 37º C.

At passages between 4 and 6, the SCs were trypsinized (Gibco), centrifuged at 1000 rpm for 7 min and seeded at a density of $2 \cdot 10^5$ cells/sample suspended in 3 µl of medium, either inside the conduit's lumen, over the bundle of PLLA fibers, or onto the films. A 5 µl Hamilton syringe (SGE Analytical Science) was used for this purpose. The HA conduits had been slightly dehydrated before seeding; in that way, the material partly swells with the injected medium and outside leakage of the cell suspension could be avoided. Four HA5 conduits were seeded on one of their outer surfaces with a micropipette at the same SCs density in order to verify if cells could penetrate through the conduits' wall. The *top side* of the conduits was meticulously avoided during this experiment, since it possessed different porosity. All samples were left incubating undisturbed in a multiwell culture plate at 37ºC at 5% CO_2 for 30 min to prevent cells from flowing out the conduits. Next, SCs culture medium was added to each well and the cells were cultured for 1, 5 and 10 days, renewing the culture medium every 2 days.

2.5. MTS viability assay

To evaluate the cell viability within the conduits, MTS or 3-(4,5-dimethylthiazol-2-yl)-5-(3-carboxymethoxyphenyl)-2-(4-sulfophenyl)-2H tetrazolium salt assays (CellTiter 96 Aqueous One Solution Cell Proliferation Assay, Promega) were carried out on samples of HA5, HA5-PLLA, HAf, PLLAf and on glass coverslips as positive controls (N=4 each). When incorporated to the cells, MTS was bioreduced by metabolically active cells at different times of culture (1, 5 and 10 days) in a rate proportional to the number of live cells in culture. After 3 hours of incubation with the reagent, the medium was removed, and its absorbance was measured with a Victor Multilabel Counter 1420 spectrophotometer (Perkin-Elmer) at 490 nm.

2.6. Flow cytometry analysis

Cell viability was assessed also with a LIVE/DEAD Cell Viability Assay kit (Life Technologies) based on plasma membrane integrity and esterase activity. Briefly, unfixed samples (control coverslips, HA5 conduits and HA5-PLLA conduits, after 5 and 10 days of cell culture) were incubated with 2 μM of calcein AM (marker for live cells) and 4 μM of ethidium homodimer-1 (EthD-1; marker for dead cells) for 30 min at room temperature. Cells in samples of HA5, HA5-PLLA and control coverslip were detached with trypsin and analyzed by flow cytometry (FC500, Beckman Coulter) measuring fluorescence emission for calcein and ethidium homodimer-1 (i.e. 530 ± 30 nm and 610 ± 20 nm band-pass, respectively). Data were analyzed by using RXP software (Beckman Coulter, Brea, CA, USA), measuring the cumulative sum of three samples for each condition and timepoint to ensure a cell population over 100000 cells (a requirement of the LIVE/DEAD kit protocol). Only cells with positive staining for calcein (bottom right region in the fluorescence scatter plot, named as LIVE cells) or for ethidium homodimer-1 (upper left, named as DEAD cells) were considered for this study. Thus, unlabeled cytometer counts (negative for calcein and ethidium homodimer-1), comprising cell debris and apoptotic cells with low esterase activity, were excluded. As for the few double-stained cells (positive for both stains), they were discarded because of the inconsistency of a cell being alive and dead simultaneously.

In order to better quantify cell fate (fraction of apoptotic, late apoptotic and necrotic cells) at each culture time, cells cultured on coverslips and in both types of conduits were stained using annexin V-FITC (Immunostep) in combination with propidium iodide (PI; Life Technologies). Samples were incubated in calcium binding buffer with annexin V-FITC 1:100 for 30 min in the dark, rinsed with PBS, suspended with PI (1 μg/ml) and, after that, the cells were immediately trypsinized and monitored with a flow

cytometer. Again, the cumulative sum of three samples was used for each factor and the percentages of viable, apoptotic and necrotic subpopulations determined after 1, 5 and 10 days of culture by means of RXP software. Quadrant A2 (upper right, annexin V+/PI+) included late apoptotic and necrotic cell populations; apoptotic cells appear in quadrant A4 (bottom right, annexin V+/PI-) displaying green fluorescence and necrotic cells in quadrant A1 (upper left, annexin V-/PI+). Although the unlabeled counts are frequently considered viable cells (quadrant A3, bottom left, annexin V-/PI-), this region inherently includes an unknown fraction of cell debris; those which are able to seep after the first FS/SS gating.

2.7. Cell morphology analysis

2.7.1. Immunocytochemistry

HA5 and HA5-PLLA conduits were rinsed with PBS after each culture time, fixed for 20 min in formaldehyde 4% w/v at room temperature, permeabilized for 30 min with blocking buffer (PBS + 1% BSA + 0.1% Tween-20), and incubated with mouse monoclonal anti-p75 (1:100 in blocking buffer, Sigma-Aldrich), rabbit anti-p0 (1:50, Abcam), rabbit anti-GFAP (1:500, Dako) or rabbit anti-s100 (ready to use, ImmunoStar) antibodies overnight at 4ºC in a humidified chamber. After rinsing in PBS, SCs inside the conduits were incubated with secondary antibodies goat anti-mouse Alexa 488 (1:200 in blocking buffer, Jackson Immunoresearch). To reveal F-actin, non-immunotreated samples were stained with BODIPY FL phallacidin (1:200 in PBS, Life Technologies) by incubating for 30 min. The nuclei of all samples were counterstained with DAPI (1:5000 in blocking buffer, Sigma). After additional washes with PBS, immunopositive SCs were observed using a multiphoton technique (FV1000 MPE, Olympus) to see them without cutting the conduits. Images by confocal laser scanning

microscopy (FV1000, Olympus) were obtained after opening the conduit in order to examine the lumen in all samples.

To follow in time the proliferation of the SCs inside the conduits, every 2 days samples were fixed and cut transversally and the cross-sections were observed in the confocal microscope, up to 11 days of cell culture.

The HA5 conduits with the SCs seeded on one of their outer faces were fixed after 5 days of culture and stained only with DAPI. In order to study the cells within the conduits, these were carefully cut with a scalpel in longitudinal sections (unless otherwise specified) after the cell fixation and staining.

In addition, some of the HA5 conduits cultured for 10 days were fixed with formaldehyde were subjected to trichrome staining. Firstly, the samples were treated with Harris' hematoxylin for 10 min and rinsed just 10 s with HCl (Sigma-Aldrich) 0.1% in absolute ethanol. The second staining was performed with a solution of Alcian Blue 8GX (Sigma-Aldrich) in acetic acid (Scharlab) 3% v/v with pH 2.5 for 30 min. After washing the conduits with cells for 1 h with tap water, they were immersed in a Picro Sirius Red Solution (Abcam). The three stains were intended to reveal cell nuclei, mucopolysaccharides and collagen I and III from the ECM secreted by the SC, respectively. To avoid excessive staining of the crosslinked HA structure of the conduits (HA is indeed a mucopolysaccharide), 3 last rinses of 15 min with acetic acid 3% v/v were conducted, and samples were left O/N in the same solution. Once stained, the samples were included for 1 h in sucrose 30% w/v to cryoprotect cells and embedded O/N in OCT (Leica). Finally, the OCT blocks were freezed at -30º C and cut each 5 μm with a CM 1520 cryostat (Leica), in order to observe the slices with a microscope (Eclipse 80i, Nikon)

2.7.2. Scanning electron microscopy

At 10 days of culture, HA5 and HA5-PLLA conduits were fixed at 37ºC during 1 h with 2.5% glutaraldehyde in PB 0.1 M, washed using the same buffer and post-fixed by immersion in 2% osmium tetroxide in PB 0.1 M for 90 min in dark. After 4 washes with distilled water at 4º C, the samples were dehydrated in a graded ethanol (30º, 50º, 70º, 96º and 100º for 10 min each). After dehydration, conducts were dried in a critical point dryer in order to exchange ethanol for CO_2. Conduits were coated with an ultrathin layer of gold and observed in a Hitachi S-4800 SEM.

2.7.3. Transmission electron microscopy

Conduits (HA5 and HA5-PLLA) cultured for 10 days were fixed with 2.5% of glutaraldehyde, postfixed with 2% osmium tetroxide, rinsed and dehydrated with increasing concentrations of ethanol. Next, samples were embedded in Araldite (Durcupan, Fluka) and polymerized at 60ºC overnight. Ultrathin sections (0.5 µm thickness) were cut (UC6, Leica) and observed under a FEI Tecnai Spirit G2 transmission electron microscope (TEM).

2.8. Image processing and statistical analysis

Image processing and analysis was done using an in-house software developed under MATLAB R2009a (The MathWorks, Inc.). A series of fluorescence microscopy images of HA5 and HA5-PLLA conduits stained with phallacidin after 10 days of culture were joined sequentially to obtain a global panoramic view of the entire conduit in length (see sketch in Figure 1D). All images were grayscaled and the central axis of the conduit was manually outlined throughout its entire length. Introducing the diameter of the channel as an input parameter (400 µm), the channel edges were calculated from the

central axis. Once the center and edges of the channel were delineated, the grey intensity value (0 – 256) of all pixels in each transversal section (Y-axis, image height) of the lumen was measured and, thus, the mean value and its standard deviation was calculated for each section throughout the conduit length. Both mean and standard deviation data from HA5 and HA5-PLLA images were normalized (up to 1) considering 0 and 1 the lowest and highest grey intensity values of the entire image, respectively.

The data collected from the MTS assay are reported as the mean ± standard deviation assuming the data are normally distributed (hypothesis proved). The statistically significant differences (with respect to control) were assessed with a confidence degree of 95% with the software Statgraphics Centurion XVI (StatPoint Technologies, Warrenton, VA) by means of the Tukey's honestly significant differences (HSD) mean comparison test after finding no relevant differences between samples variances by a one-way ANOVA study of the data. A similar procedure was applied to EWC data gathered in the immersion swelling assay, comparing samples immersed in water with those immersed in DPBS. A later ANOVA study of the swelling assay data revealed differences between the variances of the dimensional variation distributions and, therefore, three pairwise mean comparisons were performed between the groups (length, width and inner diameter).

3. Results

3.1. Conduit morphology

Soft stable conduits were obtained with dimensions 5.38 ± 0.25 mm long and 1.25 ± 0.12 mm wide, with a centered inner cylindrical channel of 0.41 ± 0.06 mm diameter (Figure 1B and 1C). This conduit length was chosen to agree with the dimensions of the striatal pathway in a rat model of Parkinson's disease, as read from Paxinos and

Watson's rat brain atlas [54]. Conduits with lengths up to 20 mm could also be produced with the same methods, but they are not shown here. The central channel was wide enough to permit insertion of 20 PLLA fibers within (Figure 1B and 2B).

The morphology of HA5 and HA5-PLLA conduits is shown in figures 1C and 2. The central channel (Figure 2C) runs from end to end the conduit (Figure 2A). In the case of HA5-PLLA conduits, the PLLA fibers (Figure 2B') are located in the interior of the channel (Figure 2B) as a bundle of loose individual fibers.

A study of the porosity in different zones of the HA5 conduits walls revealed three pore types (Figure 2C and details 2D, 2E and 2F in it). The channel inner surface (Figure 2D) had a uniform microporosity of around 1 μm size (detail in figure 2D'); the inner matrix of the wall (Figure 2E) showed honeycomb-like interconnected larger pores, and the external surface of the conduit (Figure 2F) was rough with a randomly-sized scatter of pores in the order of a few microns.

3.2. Water uptake

By means of high-contrast photographs of conduits in dry and swollen states it was possible to determine the dimensional changes of the materials upon water sorption. The swelling stretch ratios along the relevant sample dimensions (length, width, inner diameter) were almost the same, around 1.21 (Figure 3A).

The water uptake of the HA1, HA3 and HA5 conduits in dynamic swelling experiments under controlled relative humidity was recorded until reaching equilibrium, Figure. 3B. The EWC decreased with the concentration of HA in the starting solution, from 4.24 ± 0.19 for HA1 to 1.55 ± 0.03 for HA5. The diffusion coefficients of water in each HA porous matrix was determined with the slope of the linear fit of the data, according to equation 2, for a wall thickness, *e*, of 0.62 mm (inset in Figure. 3B). It was checked that

the data used for the fit satisfied $\tau = 4Dt/e^2 << 1$ and the interval $(m_t-m_0)/(m_\infty-m_0) \leq 0.6$, in which equation (2) is a proper approximation. Values of $1.478 \cdot 10^{-13}$, $1.483 \cdot 10^{-13}$, $1.679 \cdot 10^{-13}$ m^2/s, respectively, were obtained for the water diffusion coefficient of the HA1, HA3 and HA5 samples, revealing, thus, that the water sorption kinetics were alike in all the cases. Data from the swelling assay with HA3 and HA5 conduits immersed in distilled water or in DPBS revealed parallel results to those in humidified atmosphere, insofar as the ratio of the EWC for HA3 and HA5 was close to two (and 2.23/1.55 = 1.44 for HR100%). The overall EWC values, however, were 30 times higher, compared to data from Figure 3B, due to the considerable amounts of liquid lodged inside the scaffold's matrix micropores, in agreement with its porous nature as seen by SEM. No differences were found in the amount of liquid absorbed by the conduits immersed in water or in DPBS, albeit the presence of ions in the latter. The conduits with the lowest water uptake (HA5) were selected for further study with the cells.

3.3. Viability of Schwann cells in conduits and on films

The viability and proliferation of SCs cultured on HA films, on PLLA films, on coverslips, within HA5 conduits, and within HA5-PLLA conduits was assessed (Figure 4A). Absorbance in MTS assays increased with culture time for both HA and PLLA films, but with values significantly different at all times, those of the PLLA being always higher and closer to the coverslip data. In HA5 and HA5-PLLA conduits, absorbance reached higher values than in the two-dimensional HAf, having the same order of magnitude for each culture time as those found on PLLAf at day 10.

Quantitatively, flow cytometry analyses revealed an increase in the percentage of LIVE SCs for all samples, whereas the percentage of dead cells remained nearly constant over

time. There are only few discrepancies between the 3D conduits, which show a similar behavior, and the control.

Cell fate in HA5 and HA5-PLLA conduits was studied in more depth by flow cytometry using annexin V-FITC and PI, to clearly distinguish viable, apoptotic and necrotic cell populations. Figure 5A shows, as an example, two scatter plots (corresponding to a control sample and a HA5-PLLA conduit) of the fluorescence intensities read for cells stained with these reagents, both after 10 days of culture. Quadrants A1 and A2 (upper left, PI+/annexin-, and upper right, PI+/annexin+, respectively) include those cells with damage in their membranes (late apoptotic and necrotic cells) because they allow PI to go through and display red fluorescence. Apoptotic cells, as it has been already stated, appear in quadrant A4 (lower right, annexin+/PI-) displaying green fluorescence. The cytometry counts are colored according to their spatial density, from highest (red) to lowest (blue). Quantitatively, the fractions of viable cells, apoptotic cells, and necrotic cells for the HA5 conduit at 10 days were 82%, 4% and 12%, respectively, similar to the same data for the control (87%, 5% and 9%). In the case of HA5-PLLA conduits the proportion of viable cells was slightly lower: 75%, 3%, and 22%, respectively (Figure 5B).

3.4. Morphology and distribution of Schwann cells along the conduit channel

At day 10 the cells cultured inside the HA5 and HA5-PLLA conduits were immunopositive for the Schwann cell markers GFAP, p75 and S100 (Figure 6A-D'), proving the stability of their phenotype under these culture conditions. The PLLA fibers were densely covered by SCs (Figure 6A´-D'), these were aligned parallel to the fiber axis, well adhered on the PLLA, and displayed a morphology with an overall spindle shape oriented in the direction of the fiber (Figure 6G and 6H). On the lumina surfaces

of both HA5 and HA5-PLLA conduits, SCs achieved a high density after 10 days of culture, completely covering the lumen's surface (Figure 6A, D, F). Whereas SCs on coverslips were planar (Figure 6E), on the lumen's surface they exhibited a wide range of morphologies, with more bumpy shapes and tight cell-cell contacts (Figure 6F; see also Figure 7B). These morphologies on the lumina were found both for HA5 and HA5-PLLA conduits, independently of the presence of the PLLA fibers in the channels.

The seeded cells proliferated to the extent of forming a continuous gap-free tube spanning the lumen's length. At day 10 of culture a tapestry of Schwann cells had developed which coated the inner surface of the conduit's channel (Figure 7A). This tight cell mantle (Figure 7B) formed a cell cylinder which was easily detached from the channel surface when the conduits were cut for observation (Figure 7C and 7D). Trichrome staining of cyrosections of HA5 seeded conduits (Figure 7E and F) showed that the continuous layer of SCs on the lumen was approximately 20 – 35 μm thick. (collagen fibers in maroon) This thickness is also inferred from ultrastructural details of longitudinal (Figure 7G) and transversal sections (Figure 7H) seen by TEM; these further show that SCs' nuclei sections (dark grey) were elliptical in longitudinal sections, with the major axis parallel to the lumen axis, and were rounded in transversal cuts, what might suggest a bipolar spindle-like cell shape. Confocal microscope images of the conduits' cross-sections at different culture times revealed the progressive coverage of the channel's cross-sectional circumference by the proliferating SCs, showing that fully developed cell tubes had formed by day 9, and that by day 11 the tube's cross-section had a significant cell density (Figure 8). A thickness estimate based on the day 11 image in Figure 8 is agrees with the above 20-35 micron figure.

These experiments also proved the impermeability to cell diffusion of the inner channel surface, since no cell could be detected in the conduits' matrix beyond the lumen region (Figure 7A, D, E, F, and Figure S2 of the infiltration experiment.

The expression of myelin protein zero (p0) after 10 days of culture increased in comparison with day 1 (Figure 9) in HA and HA-PLLA conduits. At short culture times, the protein p0 was barely expressed and it was restricted to the perinuclear area, whereas at longer culture times this glycoprotein was more intensively expressed in the whole cytoplasm.

A more macroscopic view of the biohybrids was obtained with the help of a set of fluorescence microscopy images spanning the whole length of the conduits; the set of images was then fitted together to obtain the global reconstruction shown in Figure 10, and the intensity of color at different points of each section of the tubes was taken as an indirect measure of the cell density. The standard deviation around the mean value of the cell density shows the degree of homogeneity of the cell distribution at each cross-section. These pictures cannot distinguish the cells forming the sheath on the lumen from those adhered on the microfibers in the case of sample HA5-PLLA, and no significant difference can be deduced between both conduits. Multiphoton images (shown in Supplementary Figure S1) permitted to observe, without cutting the conduits, the continuous cell sheet coating the inner faces at one end of the lumen in HA5 and HA5-PLLA conduits.

4. Discussion

Decellularized grafts and biomaterial-based nerve conduits to regenerate nervous system pathways (especially peripheral nerves) have been proposed as a promising tool in the last decades, but results rarely show a significant improvement compared with

mere epineural suture or autografts [18,28,55], in particular for PNS human models [56] or CNS repair procedures [11,57]. Even more sophisticated and long-term *in vivo* experiments have not obtained remarkable functional restoration [9,58]. The limitations in these approaches stem from several factors, like the restrictive cell response owing to activated astrocytes and macrophages [11,28,59]. The long-gap (>4 mm) dystrophic effect, especially for neurons or axons penetrating the CNS-PNS transition zone [57,60], or the leakage or death of grafted cells before they can positively influence the environment [59,60], have been identified as key issues as well. The lack of porosity in the proposed devices, representing a barrier for the exchange of nutrients and cytokines, has been also identified as a cause of failure [63]. Here we have developed a novel biohybrid, which tries to overcome some of these drawbacks and may be of help for the reconstruction of axonal tracts in the nervous system. Instead of following the more common approach of multiple-channeled tubular scaffolds, the concept of a wider-diameter, single-channel conduit with guidance microfibers in its interior was explored. Nerve conduits based in multichannel structures [64,65] have been already used for regeneration studies of neural tracts, showing the concept to be feasible beyond the critical gap [66]. PLLA filaments have been proposed as a promising tool for axon growth and guidance [67]. A special feature of our conduit is a triple-layer porous structure, which results in a more specific pore architecture than comparable solutions [68]. The specificities of the manufacturing process account for this layered structure: the template of the conduit is formed by an outer PTFE mold and an inner PCL fiber generating the central channel. Since both PTFE and PCL are hydrophobic polymers, the water crystals that develop during lyophilization, which generate the microporosity in the conduit's cross-section, retract from the PTFE and the PCL surfaces, thus leaving at those surfaces denser strata of HA. Thus the material is left with a cross-section of

variable porosity: layers at the outer and inner surfaces with smaller porosity, and the layer in-between with a higher porosity (Figure 2D-F). The greater compactness of the lumen's surface impedes seeded SCs from spreading out of the channel, while the outer surfaces may act as a protective barrier against host inflammatory cells (our SCs did not cross the outer conduit faces, see Supplementary Figure S2). This impermeability to cells, here verified with Schwann cells, doesn't extend to molecules, however. HA is a flexible-chain polymer hydrogel, through which large molecules such as BSA diffuse with ease [69]. The porous structure permits the diffusion of nutrients, waste products, dissolved gases and cytokines or other cell cues involved in cellular communication and regulation. The negative aspect to this free exchange is that also toxic molecules from the surrounding damaged environment could penetrate the constructs[1]. How this would compromise the viability of the seeded SCs and, eventually, developing neuronal tracts is a matter which must be answered with *in vivo* experiments.

The conduit's chemical composition of hyaluronic acid polymer chains should be ideal for engraftment purposes, inasmuch as HA is a biodegradable and biocompatible extracellular matrix component with low host immune response [39,70,71]. HA oligomers, and thus HA-degradation products, can have pro- or anti-inflammatory effects depending on their molecular weight [72-74]. Actually, different reactive oxygen species involved in the degradation process lead to different chemically modified HA oligomers, which are the ones involved in inflammation [75,76]. Low molecular weight fragments of HA tend to be pro-inflammatory, whereas high-molecular weight fragments have anti-inflammatory effects [77]. Crosslinking with DVS increases the molecular weight of HA chain scission fragments, and, actually, several DVS-crosslinked HA products are approved for human use (references in the introduction).

[1] We acknowledge an anonymous referee for calling our attention to this problem.

This leads us to believe that the chemical composition of our scaffolds would raise no compatibility issues when implanted.

Even though crosslinked HA is a highly hydrophilic material [37,78], after lyophilization its swelling in aqueous solutions is only moderate and isotropic (swelling stretch ratios around 1.21 in all significant dimensions, Figure 3A). This may be an important factor to consider for its surgical implantation, since nerves and the soft tissues in the CNS are acutely sensitive to compression and this could otherwise affect the regenerative response of the host environment. Furthermore, HA is especially poor as regards cell-attachment properties, partly due to its high equilibrium water content [79]. This is reflected in the low values of absorbance of the MTS assays on HA films (Figure 4A); PLLA films, being more hydrophobic, adsorb more ECM proteins, and thus are much better cell adherents. But morphology, phenotype and general response of cells may be greatly affected by the physical characteristics of the culture environment [80]. Thus, when seeded in the curved, confining HA conduits, SCs survived and proliferated much more than on the HAf planar substrates, showing results comparable to those of the PLLA films and controls. This must be attributed to the confinement of the channel, which impedes viable but non-adhered cells to leak outside, and maybe also to the fact that the channel surface has a microporosity which is absent in HAf substrates, which had not suffered lyophilization; such a microporosity is frequently beneficial for cell attachment. The overall anti-adherent characteristics of crosslinked HA, however, may be an advantage for preventing glial scarring [39,82], since a quiescent effect of HA has been identified on human astrocytes [83,84]. The evolution with time of the ratio of viable to dead cells in the conduits (Figure 4B and Figure 5B) suggests that an initial stage dominated by the poor cell attachment typical of HA is followed by a stage of easy proliferation of the viable cells, which retained their

phenotypic markers (Figure 6). The presence of the PLLA fibers made no significant difference in this respect.

The morphology of the Schwann cells on the different substrates showed remarkable differences. The cells on the planar substrates (films and coverslips) are flat (Figure 6E); on the PLLA fibers they appeared bulkier, bipolar and oriented (Figure 6H), and within the HA5 and HA5-PLLA conduits they tightly aggregated forming a continuous layer, where multipolar morphologies coexisted with more rounded ones (Figures 6F and 7B). The presence of fibers itself in the conduits did not translate into an increased cell proliferation.

A most remarkable result of the cell culture within the scaffolds was the fact that the conduits organized the growth of the cell population into a new kind of cellular structure. After 10 days of culture the seeded cells had proliferated to such a degree that they tightly covered the whole inner surface of the conduit's channel forming a continuous cylindrical mantle, with no visible gaps between the cells (Figure 7). This sheath-like structure extended uniformly along the whole length of the conduit. The cell sheath had a variable thickness between 20 and 35 microns (Figure 7F, Figure 8), and detached easily from the channel surface when this was cut (Figure 7C and 7D). Thus, the conduit material acted as a template for the development of macroscopic Schwann-cell cylinders, a cellular structure which hasn't been reported earlier. Such a confluent cell layer was unable to form on the planar crosslinked HA substrates. A number of factors of the cell-biomaterial interaction must have combined in order to give rise to this singular structure. First of all, the HA environment is friendly enough for the cells to sustain their proliferation; secondly, the hydrophilicity of the channel surface makes cell-cell interactions to be preferred over cell-material ones, thus promoting the tight, gap-free cell-cell junctions, instead of an attachment of the cells on the material's

surface; thirdly, the channel curvature constrains the possibilities of spatial growth of the proliferating cells, forcing them to fold following the cylinder geometry, as can be seen from the temporal sequence shown in Figure 8. Finally, the large diameter of the single channel was probably what allowed the high proliferation rate needed for the development of this macroscopic structure. Therefore, the synergy between the channel's geometry and the material's anti-adherent properties leads to the formation of this Schwann-cell macroscopic sheath. At the same time, the viable development of this structure within a channel of considerable length testimonies to the unhindered flow of nutrients, proteins and all other vital molecules through the conduit's wall pores, as well as to the ability of the channel's walls to impede cells leaking outwards.

The presence of the PLLA fibers did not affect the development of this sheath in the conduits. In HA-PLLA scaffolds part of the seeded cells grew on the fibers, while the remaining cells on the lumina proliferated and organized into the cell-tube. In all cases, the cells forming the sheath behaved has mature Schwann cells, expressing common SCs markers (GFAP, p75, S100). In addition, they produced glycoprotein p0, which comprises the major protein in myelin (making up more than 50% mass of myelin sheath) and mediates membrane adhesion in the spiral wraps. The protein p0 was barely detectable after day 1 but its expression was massive after 10 days in cells cultured on both type of conduits. Although the SCs p0 expression has been formerly considered inherent to axonal signaling [85], its expression has been proved to be constitutive for SCs under certain conditions even in absence of axons [86]. A significant increase in p0 may support the effective regeneration of nervous tracts after lesions [87]. Thus, the p0 synthesis stimulation might represent an additional benefit of the present conduits for axonal pathway regeneration.

Given the supportive role of Schwann cells for axon outgrowth in the PNS, the biohybrid tubular structures here developed could find application in strategies seeking to reconnect neuronal populations across long distances both in the central and the peripheral nervous systems. Neuronal precursors should be combined with the biohybrid here presented; the Schwann cells preseeded in them would act as neurotrophic factor pumps and as a reservoir of accompanying cells for the outgrowing axons. In previous studies we found that scaffolds implanted in the brain of rats became vascularized; blood vessels developed inside channels with diameters of 90 microns from endothelial cell precursors that had migrated into the empty scaffold [88]. The lumina of the present constructs are much wider, and thus invasion by vessel precursors should be easier. Moreover, it has been found that Schwann cells secrete VEGF and are instrumental in differentiating endothelial cell precursors to blood vessels: the geometrical lay-out of nerves becomes a template for patterning the development of the arterial network [89-91]. It is thus expected that, once implanted, our constructs would be easily vascularized, ensuring early as well as long-term viability of the biohybrid. Of course, confirmation of these hypothesis must wait for further results with *in vitro* co-cultures and *in vivo* experiments.

5. Conclusions

Tubular HA conduits have been developed with a layered pore distribution along their cross-section which prevents cell leakage from within and cell invasion from the outside, while allowing unrestricted nutrient and molecules diffusion. The HA5 conduits possess structural stability and a sensibly restricted swelling degree in physiological medium when compared to HA1 and HA3 conduits. The conduits' lumina constitute a space where cells of interest could be hosted in a protected manner for

transplantation. A bundle of PLLA fibers is incorporated in the lumen to help guided cell growth and eventually axon sprouting. The conduits have proved to sustain viable Schwann cell cultures in their whole length, improving viability and distribution with respect to planar cell-friendly substrates such as PLLA, despite the marked low-adherent characteristic of HA that usually prevents a good cell proliferation. When cultured within the conduits, SCs proliferated until coalescence and then developed as a tight mantle adapted to the inner cylindrical surface of the channel that spanned the whole length of the conduit (6 mm) without loss of continuity. SCs thus grown kept their phenotypic characteristics and produced substantial amounts of the myelin constitutive protein p0 over time even in the absence of neurons. The development of these synthetically engineered macroscopic cell cylinders is the outcome of the interplay of cell proliferation in a friendly but non-adherent environment and a suitably sized and shaped confining geometry. These novel porous HA conduits and the biohybrids obtained when Schwann cells are grown within them seem promising tools in strategies to restore damaged neural tracts. Their combination with co-cultures of neurons and neuronal progenitor cells is under study.

Acknowledgements

The authors acknowledge financing through projects MAT2011-28791-C03-02 and 03, and ERA-NET NEURON project PRI-PIMNEU-2011-1372. We thank the Cytomics Core Facility at Príncipe Felipe Research Center (CIPF, Valencia, Spain) for their support and advice in flow cytometry experiments, and the Electron Microscopy Service at the UPV, where the SEM images were obtained.

References

[1] Fawcett JW, Keynes RJ. Peripheral nerve regeneration. Annu Rev Neurosci 1990; 13:43-60.

[2] Gil-Perotín S, Alvarez-Buylla A, García-Verdugo JM. Identification and characterization of neural progenitor cells in the adult mammalian brain. Adv Anat Embryol Cell Biol 2009; 203:1-101, ix.

[3] Yamashita T1, Ninomiya M, Hernández Acosta P, García-Verdugo JM, Sunabori T, Sakaguchi M, et al. Subventricular zone-derived neuroblasts migrate and differentiate into mature neurons in the post-stroke adult striatum. J Neurosci 2006; 26:6627-6636.

[4] Ramón y Cajal S. Degeneration and regeneration of the nervous system. Oxford University Press, editor. London, 1928.

[5] Hilton M, Middleton G, Davies AM. Bcl-2 influences axonal growth rate in embryonic sensory neurons. Curr Biol 1997; 7:798-800.

[6] Goldberg JL, Klassen MP, Hua Y, Barres BA. Amacrine-signaled loss of intrinsic axon growth ability by retinal ganglion cells. Science 2002; 296:1860-1864.

[7] Fawcett JW, Asher RA. The glial scar and central nervous system repair. Brain Res Bull 1999; 49:377-391.

[8] Hudson TW, Evans GR, Schmidt CE. Engineering strategies for peripheral nerve repair. Clin Plast Surg 1999; 26:617–628.

[9] Strauch B, Ferder M, Lovelle-Allen S, Moore K, Kim DJ, Llena J. Determining the maximal length of a vein conduit used as an interposition graft for nerve regeneration. J Reconstr Microsur 1996; 12:521–527.

[10] Moore MJ, Friedman JA, Lewellyn EB, Mantila SM, Krych AJ, Ameenuddin S, et al. Multiple-channel scaffolds to promote spinal cord axon regeneration. Biomaterials 2006; 27:419-429.

[11] Elias PZ, Spector M. Implantation of a collagen scaffold seeded with adult rat hippocampal progenitors in a rat model of penetrating brain injury. J Neurosci Meth 2012; 209:199-211.

[12] Armati PJ, Mathey EK. An update on Schwann cell biology – Immunomodulation, neural regulation and other surprises. J Neurol Sci 2013; 333:68-72.

[13] Taylor JS, Bampton ET. Factors secreted by Schwann cells stimulate the regeneration of neonatal retinal ganglion cells. J Anat 2004; 204:25-31.

[14] Bunge RP. 1994. The role of the Schwann cell in trophic support and regeneration. J Neurol 1994; 242:S19–S21.

[15] Bunge RP. Expanding roles for the Schwann cell: ensheathment, myelination, trophism and regeneration. Curr Opin Neurobiol 1993;3:805-9.

[16] Lakatos A, Franklin RJ, Barnett SC. Olfactory ensheathing cells and Schwann cells differ in their in vitro interactions with astrocytes. Glia 2000; 32:214-225.

[17] Brushart TM, Aspalter M, Griffin JW, Redett R, Hameed H, Zhou C, et al. Schwann cell phenotype is regulated by axon modality and central–peripheral location, and persists in vitro. Exp Neurol 2013; 247:272-281.

[18] Rodríguez FJ, Verdú E, Ceballos D, Navarro X. Nerve guides seeded with autologous schwann cells improve nerve regeneration. Exp Neurol 2000; 161:571-584.

[19] Ikeda M, Uemura T, Takamatsu K, Okada M, Kazuki K, Tabata Y, et al. Acceleration of peripheral nerve regeneration using nerve conduits in combination with induced pluripotent stem cell technology and a basic fibroblast growth factor drug delivery system. J Biomed Mater Res A 2013; 247:272-281.

[20] Bunge RP. Expanding roles for the Schwann cell: ensheathment, myelination, trophism and regeneration. Curr Opin Neurobiol 1993; 3:805-9.

[21] Li Y, Raisman G. Schwann cells induce sprouting in motor and sensory axons in the adult rat spinal cord. J Neurosci 1994; 14:4050-63.

[22] David S, Aguayo AJ. Axonal elongation into peripheral nervous system "bridges" after central nervous system injury in adult rats. Science 1981; 214:931-3.

[23] Takami T, Oudega M, Bates ML, Wood PM, Kleitman N, Bunge MB. Schwann cell but not olfactory ensheathing glia transplants improve hindlimb locomotor performance in the moderately contused adult rat thoracic spinal cord. J Neurosci 2002; 22(15):6670-81.

[24] Franklin RJ, Barnett SC. Do olfactory glia have advantages over Schwann cells for CNS repair? J Neurosci Res 1997; 50:665-72.

[25] Bunge MB. Bridging the transected or contused adult rat spinal cord with Schwann cell and olfactory ensheathing glia transplants. Prog Brain Res 2002;137:275-82.

[26] Cai S, Shea GK, Tsui AY, Chan YS, Shum DK. Derivation of clinically applicable schwann cells from bone marrow stromal cells for neural repair and regeneration. CNS Neurol Disord Drug Targets 2011; 10(4):500-8.

[27] Fouad K, Schnell L, Bunge MB, Schwab ME, Liebscher T, Pearse DD. Combining Schwann cell bridges and olfactory-ensheathing glia grafts with chondroitinase promotes locomotor recovery after complete transection of the spinal cord. J Neurosci 2005; 25:1169-1178.

[28] Xu XM, Guénard V, Kleitman N, Bunge MB. Axonal regeneration into Schwann cell-seeded guidance channels grafted into transected adult rat spinal cord. J Comp Neurol 1995; 351:145-160.

[29] Kallur T, Darsalia V, Lindvall O, Kokaia Z. Human fetal cortical and striatal neural stem cells generate region-specific neurons in vitro and differentiate extensively to

neurons after intrastriatal transplantation in neonatal rats. J Neurosci Res 2006; 84:1630-1644.

[30] Hicks AU, Lappalainen RS, Narkilahti S, Suuronen R, Corbett D, Sivenius J, et al. Transplantation of human embryonic stem cell-derived neural precursor cells and enriched environment after cortical stroke in rats: cell survival and functional recovery. Eur J Neurosci 2009; 29:562-574.

[31] Azanchi R, Bernal G, Gupta R, Keirstead HS. Combined demyelination plus Schwann cell transplantation therapy increases spread of cells and axonal regeneration following contusion injury. J Neurotraum 2004; 21:775-788.

[32] Liang Y, Walczak P, Bulte JW. The survival of engrafted neural stem cells within hyaluronic acid hydrogels. Biomaterials 2013; 34:5521-5529.

[33] Wang T, Spector M. Development of hyaluronic acid-based scaffolds for brain tissue engineering. Acta Biomater 2009; 5:2371–2384.

[34] Ma J, Tian WM, Hou SP, Xu QY, Spector M, Cui FZ. An experimental test of stroke recovery by implanting a hyaluronic acid hydrogel carrying a Nogo receptor antibody in a rat model. Biomed Mater 2007; 2:233-240.

[35] Tian WM, Hou SP, Ma J, Zhang CL, Xu QY, Lee LS, et al. Hyaluronic acid-poly-D-lysine-based three-dimensional hydrogel for traumatic brain injury. Tissue Eng 2005; 11:513-525.

[36] Seidlits SK, Khaing ZZ, Petersen RR, Nickels JD, Vanscoy JE, Shear JB, et al. The effects of hyaluronic acid hydrogels with tunable mechanical properties on neural progenitor cell differentiation. Biomaterials 2010; 31:3930-3940.

[37] Lam J, Truong NF, Segura T. Design of cell-matrix interactions in hyaluronic acid hydrogel. Acta Biomater 2013; 10:1571-1580.

[38] Abdalla S, Makhoul G, Duong M, Chiu RC, Cecere R. Hyaluronic acid-based hydrogel induces neovascularization and improves cardiac function in a rat model of myocardial infarction. Interact Cardiovasc Thorac Surg 2013; 17:767-772.

[39] Lin CM, Lin JW, Chen YC, Shen HH, Wei L, Yeh YS, et al. Hyaluronic acid inhibits the glial scar formation after brain damage with tissue loss in rats. Surg Neurol 2009; 72 Suppl 2:S50-54.

[40] Wei YT, He Y, Xu CL, Wang Y, Liu BF, Wang XM, et al. Hyaluronic acid hydrogel modified with nogo-66 receptor antibody and poly-L-lysine to promote axon regrowth after spinal cord injury. J Biomed Mater Res B Appl Biomater 2010; 95:110-117.

[41] Lapcík L Jr and L, Lapcík L, De Smedt S, Demeester J, Chabrecek P. Hyaluronan: preparation, structure, properties, and applications. Chem Rev 1998; 98:2663-2684.

[42] Wang X, He J, Wang Y, Cui FZ. Hyaluronic acid-based scaffold for central neural tissue engineering. Interface Focus 2012; 2:278-291.

[43] Collins MN, Birkinshaw C. Comparison of the effectiveness of four different crosslinking agents with hyaluronic acid hydrogel films for tissue-culture applications. J Appl Polym Sci 2007; 104:3183-3191.

[44] Shu XZ, Liu Y, Luo Y, Roberts MC, Prestwich GD. Disulfide cross-linked hyaluronan hydrogels. Biomacromol 2002; 3:1304-1311.

[45]West JD, Stamm CE, Brown HA, Justice SL, Morano KA. Enhanced toxicity of the protein cross-linkers divinyl sulfone and diethyl acetylenedicarboxylate in comparison to related monofunctional electrophiles. Chem Res Toxicol 2011; 24:1457-9.

[46] Ibrahim S, Kang QK, Ramamurthi A. The impact of hyaluronic acid oligomer content on physical, mechanical, and biologic properties of divinyl sulfone-crosslinked hyaluronic acid hydrogels. J Biomed Mater Res A 2010; 94:355-70.

[47] Kim JT, Choi JH, Lee DY. Pyrogenicity of hyaluronic acid hydrogel cross-linked by divinyl sulfone for soft tissue augmentation. Natural Science 2010; 2:764-768.

[48] Larsen NE, Dursema HD, Pollak CT, Skrabut EM. Clearance kinetics of a hylan-based viscosupplement after intra-articular and intravenous administration in animal models. J Biomed Mater Res B Appl Biomater 2012; 100:457-62.

[49] Schanté C, Zuber G, Herlin C, Vandamme TF. Chemical modifications of hyaluronic acid for the synthesis of derivatives for a broad range of biomedical applications. Carbohydrate Polymers 2011; 86:469–489.

[50] Lai JY. Relationship between structure and cytocompatibility of divinyl sulfone cross-linked hyaluronic acid. Carbohydr Polym 2014; 101:203-12.

[51] Conrozier T, Mathieu P, Schott AM, Laurent I, Hajri T, Crozes P, Grand P, Laurent H, Marchand F, Meignan F, Noel E, Rozand Y, Savoye JF, Vignon E. Factors predicting long-term efficacy of Hylan GF-20 viscosupplementation in knee osteoarthritis. Joint Bone Spine 2003; 70:128-33.

[52] Sun SF, Chou YJ, Hsu CW, Chen WL. Hyaluronic acid as a treatment for ankle osteoarthritis. Curr Rev Musculoskelet Med 2009; 2:78-82.

[53] Ritgen PL, Peppas NA. A simple equation for description of solute release I. Fickian and non-Fickian release from non-swellable devices in the form of slabs, spheres, cylinders or discs. J Control Release 1987; 5:23-36.

[54] Paxinos, G., Watson, C., 2007. The Rat Brain in Stereotaxic Coordinates, 6th Edition. Elsevier Academic Press, San Diego.

[55] Whitlock EL, Tuffaha SH, Luciano JP, Yan Y, Hunter DA, Magill CK, et al., Processed allografts and type I collagen conduits for repair of peripheral nerve gaps. Muscle Nerve 2009; 39:787-799.

[56] Moore AM, Kasukurthi R, Magill CK, Farhadi HF, Borschel GH, Mackinnon SE. Limitations of Conduits in Peripheral Nerve Repairs. Hand 2009; 4:180-186.

[57] Tang XQ, Cai J, Nelson KD, Peng XJ, Smith GM. Functional repair after dorsal root rhizotomy using nerve conduits and neurotrophic molecules. Eur J Neurosci 2004; 20:1211-1218.

[58] Matsumoto K, Ohnishi K, Kiyotani T, Sekine T, Ueda H, Nakamura T, et al. Peripheral nerve regeneration across an 80-mm gap bridged by a polyglycolic acid (PGA)–collagen tube filled with laminin-coated collagen fibers: a histological and electrophysiological evaluation of regenerated nerves. Brain Res 2000; 868:315-328.

[59] Mosahebi A, Fuller P, Wiberg M, Terenghi G. Effect of allogeneic Schwann cell transplantation on peripheral nerve regeneration. Exp Neurol 2002; 173:213-223.

[60] Bloch J, Fine EG, Bouche N, Zurn AD, Aebischer P. Nerve growth factor- and neurotrophin-3-releasing guidance channels promote regeneration of the transected rat dorsal root. Exp Neurol 2001; 172:425–432.

[61] Emgård M, Hallin U, Karlsson J, Bahr BA, Brundin P, Blomgren K. Both apoptosis and necrosis occur early after intracerebral grafting of ventral mesencephalic tissue: a role for protease activation. J Neurochem 2003; 86:1223-1232.

[62] Pearse DD, Sanchez AR, Pereira FC, Andrade CM, Puzis R, Pressman Y, et al. Transplantation of Schwann cells and/or olfactory ensheathing glia into the contused spinal cord: Survival, migration, axon association, and functional recovery. Glia 2007; 55:976-1000.

[63] Kim DH, Connolly SE, Zhao S, Beuerman RW, Voorhies RM, Kline DG. Comparison of macropore, semipermeable, and nonpermeable collagen conduits in nerve repair. J Reconstr Microsurg 1993, 9:415-420.

[64] Bozkurt A, Lassner F, O'Dey D, Deumens R, Böcker A, Schwendt T, et al. The role of microstructured and interconnected pore channels in a collagen-based nerve guide on axonal regeneration in peripheral nerves. Biomaterials 2012; 33:1363–75.

[65] Ngo TTB, Waggoner PJ, Romero A, Nelson KD, Eberhart RC, Smith GM. Poly(L-lactide) microfilaments enhance peripheral nerve regeneration across extended nerve lesions. J Neurosci Res 2003; 72:227–38.

[66] Matsumoto K, Ohnishi K, Kiyotani T, Sekine T, Ueda H, Nakamura T, et al. Peripheral nerve regeneration across an 80-mm gap bridged by a polyglycolic acid (PGA)-collagen tube filled with laminin-coated collagen fibers: A histological and electrophysiological evaluation of regenerated nerves. Brain Res 2000; 868:315–28.

[67] Wang HB, Mullins ME, Cregg JM, Hurtado A, Oudega M, Trombley MT, Gilbert RJ. Creation of highly aligned electrospun poly-L-lactic acid fibers for nerve regeneration applications. J Neural Eng 2009; 6:016001.

[68] Sakai Y, Matsuyama Y, Takahashi K, Sato T, Hattori T, Nakashima S, et al. New artificial nerve conduits made with photocrosslinked hyaluronic acid for peripheral nerve regeneration. Biomed Mater Eng 2007; 17:191-197.

[69] Shenoy V, Rosenblatt J. Diffusion of macromolecules in collagen and hyaluronic acid, rigid-rod-flexible polymer, composite matrices. Macromolecules 1995;28:8751-8758.

[70] Weigel PH, Fuller GM, LeBoeuf RD. A model for the role of hyaluronic acid and fibrin in the early events during the inflammatory response and wound healing. J Theor Biol 1986; 119: 219-234.

[71] Friedman PM, Mafong EA, Kauvar AN, Geronemus RG. Safety data of injectable nonanimal stabilized hyaluronic acid gel for soft tissue augmentation. Dermatol Surg 2002; 28:491-494.

[72] Stern R, Asari AA, Sugahara KN. Hyaluronan fragments: an information-rich system. European Journal of Cell Biology 2006; 85(8) 699–715.

[73] West DC, Kumar S. The effect of hyaluronate and its oligosaccharides on endothelial cell proliferation and monolayer integrity. Experimental Cell Research 1989; 183(1) 179–96.

[74] Jiang D, Liang J, Noble PW. Hyaluronan in tissue injury and repair. Annual Review of Cell and Developmental Biology 2007; 23 435–61.

[75] McNeil JD, Wiebkin OW, Betts WH, Cleland LG. Depolymerisation products of hyaluronic acid after exposure to oxygen-derived free radicals. Annals of the Rheumatic Diseases 1985; 44(11) 780–9.

[76] Lawwill T. Three major pathologic processes caused by light in the primate retina: a search for mechanisms. Transactions of the American Ophthalmological Society 1982; 80 517–79.

[77] Rayahin JE, Buhrman JS, Zhang Y, Koh TJ, Gemeinhart RA. High and low weight hyaluronic acid differentially influence macrophage activation. ACS Biomater. Sci. Eng. 2015; 1: 481−493.

[78] Larsen NE, Balazs EA. Drug delivery systems using hyaluronan and its derivatives. Adv Drug Deliv Rev 1991; 7:279-293.

[79] Arnal-Pastor M, Martínez Ramos C, Pérez Garnés M, Monleón Pradas M, Vallés Lluch A. Electrospun adherent-antiadherent bilayered membranes based on cross-linked hyaluronic acid for advanced tissue engineering applications. Mater Sci Eng C Mater Biol Appl 2013; 33:4086-4093.

[80] Shenoy V, Rosenblatt J. Diffusion of macromolecules in collagen and hyaluronic acid, rigid-rod-flexible polymer, composite matrices. Macromolecules 1995;28:8751-8758

[81] Baker BM, Chen CS. Deconstructing the third dimension: how 3D culture microenvironments alter cellular cues. J Cell Sci 2012; 125:3015-3024.

[82] Khaing ZZ, Milman BD, Vanscoy JE, Seidlits SK, Grill RJ, Schmidt CE. High molecular weight hyaluronic acid limits astrocyte activation and scar formation after spinal cord injury. J Neural Eng 2011;8:046033 (12pp)

[83] Sherman LS, Struve JN, Rangwala R, Wallingford NM, Tuohy TM, Kuntz C 4th. Hyaluronate-based extracellular matrix: Keeping glia in their place. Glia 2002; 38:93-102.

[84] Placone AL, McGuiggan PM, Bergles DE, Guerrero-Cazares H, Quiñones-Hinojosa A, Searson PC. Human astrocytes develop physiological morphology and remain quiescent in a novel 3D matrix. Biomaterials 2015; 42:134-143.

[85] Lee MJ, Brennan A, Blanchard A, Zoidl G, Dong Z, Tabernero A, et al. P0 is constitutively expressed in the rat neural crest and embryonic nerves and is negatively and positively regulated by axons to generate non-myelin-forming and myelin-forming Schwann cells, respectively. Mol Cell Neurosci 1997; 8:336-350.

[86] Cheng L, Mudge AW. Cultured Schwann cells constitutively express the myelin protein P0. Neuron 1996; 16:309-319.

[87] Schweitzer J, Becker T, Becker CG, Schachner M. Expression of protein zero is increased in lesioned axon pathways in the central nervous system of adult zebrafish. Glia 2003; 41:301-317.

[88] Martínez-Ramos C, Vallés-Lluch A, Verdugo JM, Ribelles JL, Barcia Albacar JA, Orts AB, Soria López JM, Pradas MM. Channeled scaffolds implanted in adult rat brain. J Biomed Mater Res A 2012; 100:3276-86.

[89] Mukouyama YS, Shin D, Britsch S, Taniguchi M, Anderson DJ. Sensory nerves determine the pattern of arterial differentiation and blood vessel branching in the skin. Cell 2002; 109:693-705.

[90] Li W, Kohara H, Uchida Y, James JM, Soneji K, Cronshaw DG, Zou YR, Nagasawa T, Mukouyama YS. Peripheral nerve-derived CXCL12 and VEGF-A regulate the patterning of arterial vessel branching in developing limb skin. Dev Cell 2013; 24:359-71.

[91] Carmeliet P. Blood vessels and nerves: common signals, pathways and diseases. Nat Rev Genet 2003; 4:710-20.

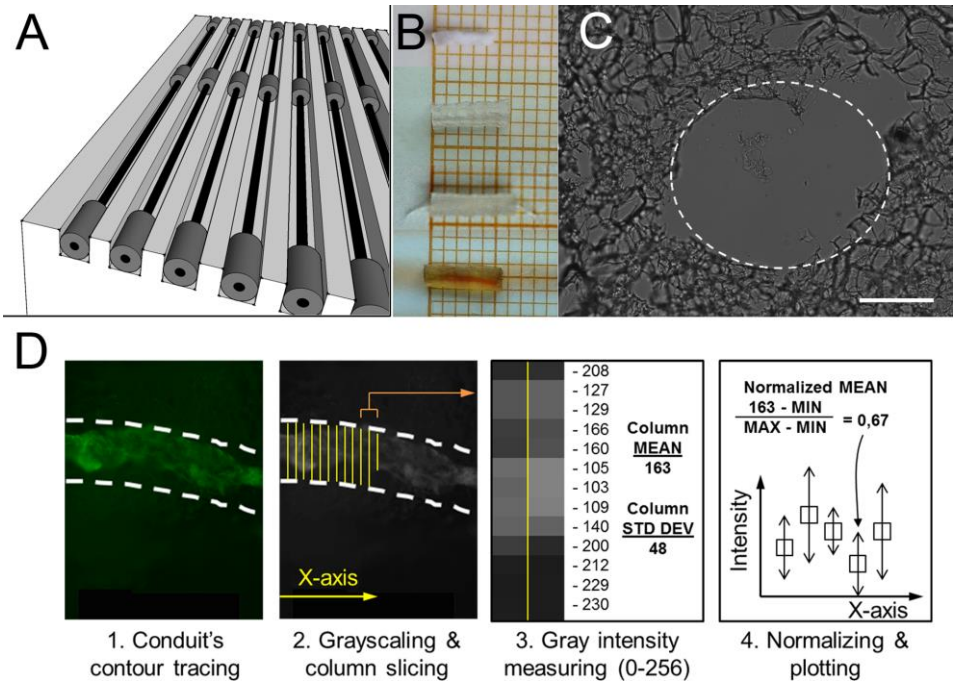

Figure 1. (A) Sketch of the PTFE mould (white) with PCL fibers (black) and PTFE washers (grey) in the grooves. **(B)** Macroscopic appearance of the conduits in different states, from top to bottom: dry after lyophilization, hydrated, hydrated with 20 PLLA fibers in the channel, hydrated and with the channel stained with reddish dye. **(C)** Bright field photograph of a cross-section of a conduit with the central channel highlighted with a dashed line. **(D)** Sketch of the method used for the digitalization of the color intensity leading to Figure 10. Scale bar = 200 μm.

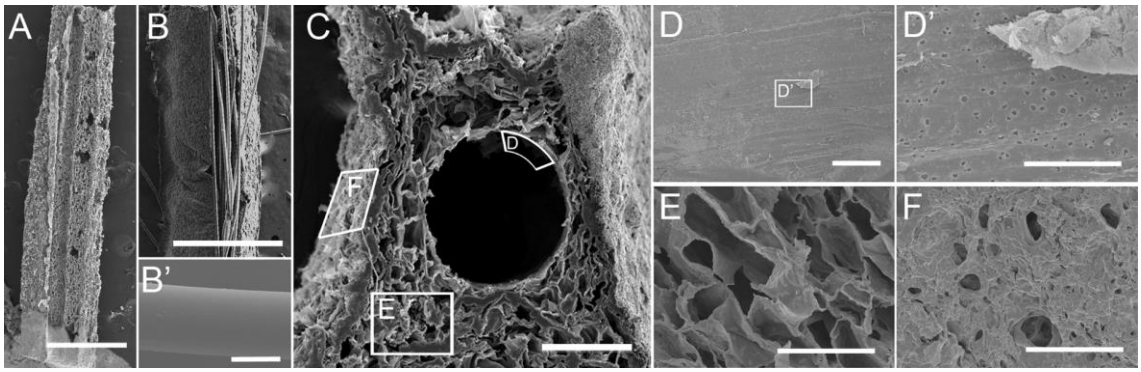

Figure 2. SEM images of longitudinal cuts of a HA5 **(A)** and a HA5-PLLA conduit **(B)**, with a detail of a PLLA fibre **(B')**. SEM image of a transversal section of a HA5 conduit **(C)**, and selected regions in it: channel surface **(D)**, conduit's outer surface **(F)**, and porous matrix of the conduit's wall of the conduit **(E)**. **(D')** is a detail to reveal the porosity of the channel surface. Scale bar = 1 cm **(A, B)**, 200 μm **(C)**, 50 μm **(D, E, F)**, 20 μm **(B')** and 10 μm **(D')**.

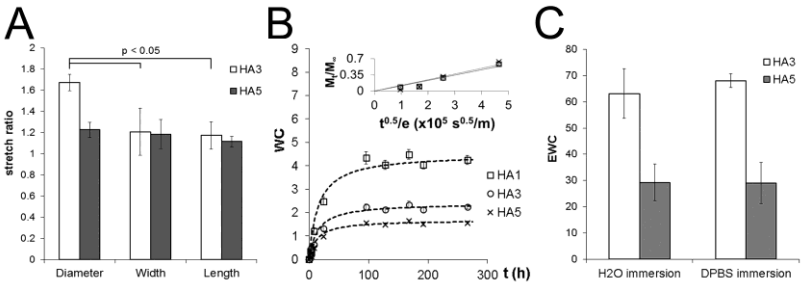

Figure 3. Water uptake of the conduits and dimensional change. **(A)** Stretch ratio of the HA5 conduit's characteristic linear dimensions (width, lumen diameter and length). Statistically significant differences are expressed with bars (N = 8, 95% confidence degree). **(B)** Water content of HA1, HA3 and HA5 conduits at different times. **(C)** Equilibrium water content of HA3 and HA5 conduits immersed in distilled water or DPBS. Inset: linear fit of data to equation 2 for the calculation of diffusion coefficients.

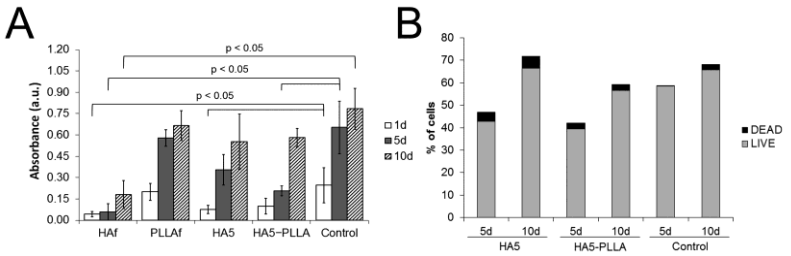

Figure 4. Schwann cells viability and proliferation. **(A)** MTS viability assays on SCs cultures on planar substrates (HAf, PLLAf and control) and in HA5 and HA5-PLLA conduits at different culture times (1, 5 and 10 days). Statistically significant differences with respect to control for the same culture time are represented with bars (N = 4, 95% confidence degree). **(B)** Cytometry data of LIVE and DEAD cells for HA5 or HA5-PLLA conduits or control after 5 and 10 days of cell culture. Glass coverslips were used as control. The missing percentage of cells up to 100% corresponds to upper right and bottom left regions of the fluorescence scatter plot.

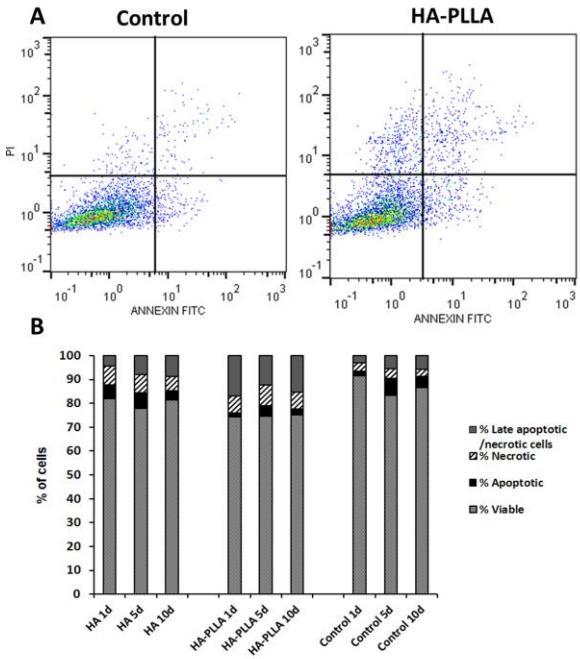

Figure 5. (A) Cytometry scatter plot for annexin V–PI cell staining after 10 days of SCs culture on a coverslip (left) and in HA5-PLLA conduits (right). **(B)** Stacked percentage chart of annexin V - PI cytometry data of necrotic, apoptotic and viable (live) cells within HA5 or HA5-PLLA conduits or on coverslips (control) after 1, 5 and 10 days of SCs culture. Both necrotic and late apoptotic cells are considered here as necrotic.

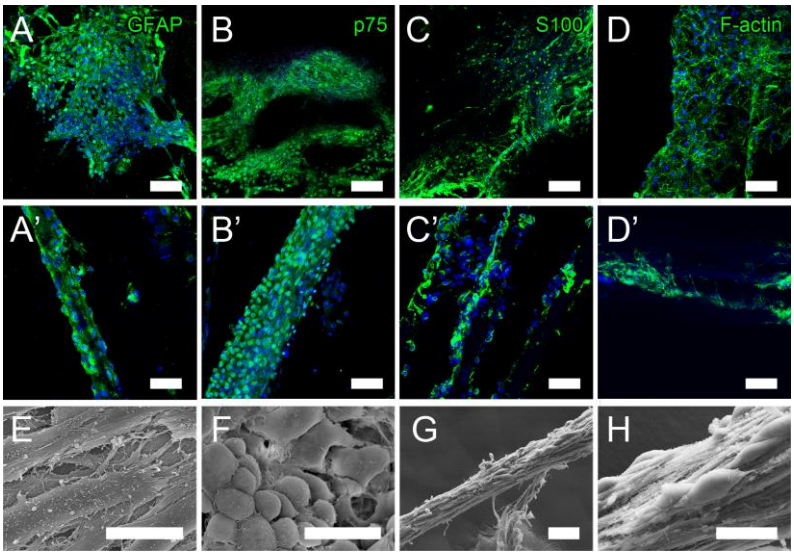

Figure 6. Confocal microscopy images of immunocytochemistry and phallacidin stainings (green) revealing expression of GFAP **(A, A')**, p75 **(B, B')**, S-100 proteins **(C, C')** and F-actin **(D, D')** in longitudinal cuts of HA5 **(A - D)** and HA5-PLLA conduits **(A' - D')**. Nuclei were stained with DAPI (blue). SEM images of SCs cultured for 10 days on coverslips **(E)**, in the lumen of a HA5 conduit **(F)** and on a PLLA fiber from a HA5-PLLA conduit **(G, H)**. Scale bar = 100 µm **(A - D)**, 50 µm **(A' - D', G)** and 20 µm **(E, F, H).**

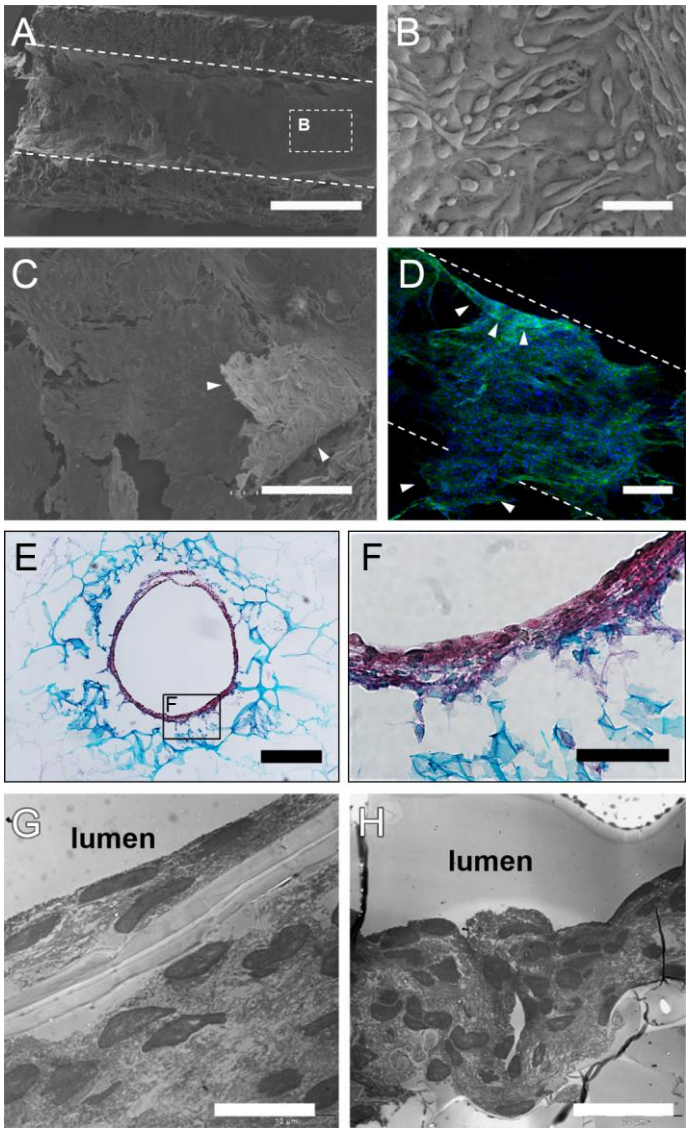

Figure 7. Schwann cell cylindrical sheets developed inside the conduit's channel. **(A)** SEM image from a longitudinal cut of the macroscopic SCs tubular sheet inside a HA5 conduit after 10 days of culture. **(B)** Details of the sheath cell distribution and organization. **(C)** SEM image of partial view of a sheet detached from the HA5 conduit, keeping its structural integrity. **(D)** Confocal microscopy image of the SCs sheet stained with phallacidin (green) and DAPI (blue). Arrowheads delimit the boundary of the detached part of the sheet. **(E, F)** Transversal cryosections of HA5 conduits cultured for 10 days with SCs in their lumen after staining with Harris' hematoxylin, alcian blue and picrosirius red. No SCs were detected inside the porous matrix of the HA conduit wall (cyan). **(G, H)** TEM images of longitudinal **(G)** and transversal **(H)** sections of the cell sheet layer in HA5 conduits for the same culture time. Nuclei seen in dark grey. The limits of the conduit's channel are traced with dashed lines in **(A, D)**. Scale bar = 500 µm **(A)**, 200 µm **(B, C, E)**, 50 µm **(D, F)**, 20 µm **(H)** and 10 µm **(G)**.

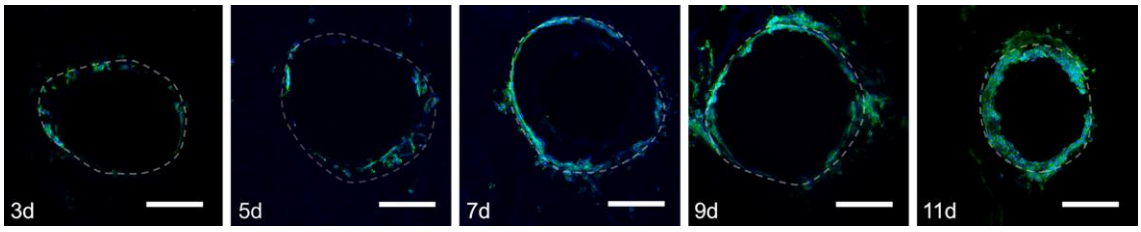

Figure 8. Confocal microscopy images of transverse cross-sections of the HA5 construct after 1, 3, 5, 7, 9 and 11 days of SCs culture. Cells' cytoskeleton, stained in green with phallacidin, and nuclei, stained in blue with DAPI, allow following the development of the cylindrical cell-sheets over time, shaped by the conduit's channel. Scale bar = 200 μm.

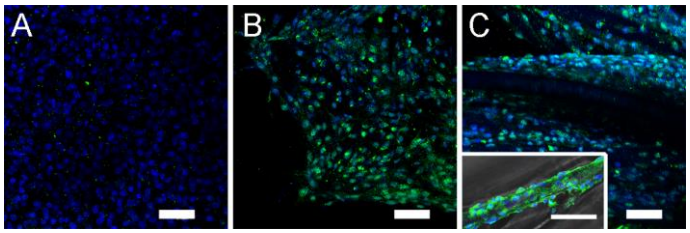

Figure 9. Expression of p0 protein. Confocal microscopy images of SCs cultured for 1 **(A)** and 10 days **(B, C)** in HA5 **(A, B)** and HA5-PLLA conduits cut longitudinally **(C)**, immunostained to reveal p0 protein (green). Cell nuclei stained with DAPI (blue). Detail in the lower left corner of **(C)** shows a single PLLA fiber extracted from the HA5-PLLA conduit at the same culture time. Scale bar = 50 μm **(A, B, C, detail)**.

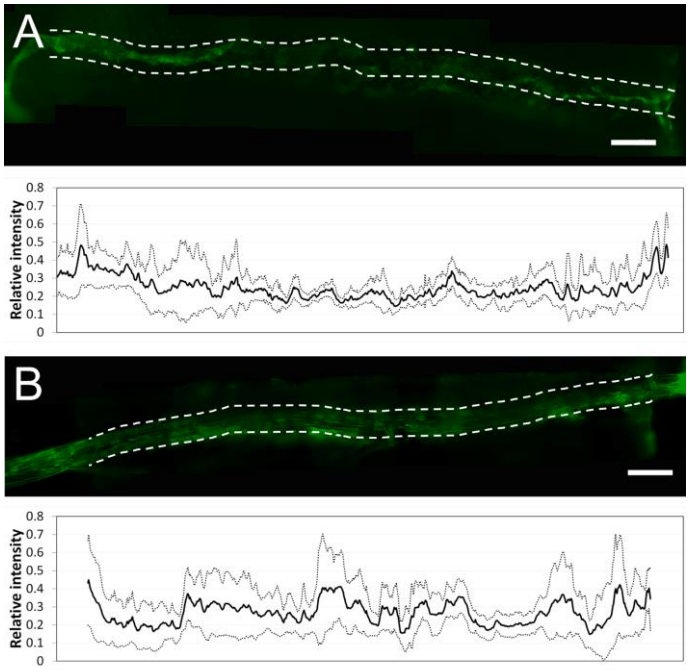

Figure 10. Compound panel spanning the conduit's complete length, made from a series of fluorescence microscopy images of longitudinal sections of the HA5 **(A)** and

HA5-PLLA conduits **(B)**, after 10 days of SCs culture. F-actin stained in green by phallacidin. Below both panels: plots of the normalized mean values (dark curve) of the intensity of the grey at each section along the lumen's axis and of the standard deviation for each section (lighter grey curves), see text in section 2.8. Dashed white lines demarcate channel limits used as input by the software. Scale bar = 500 μm.

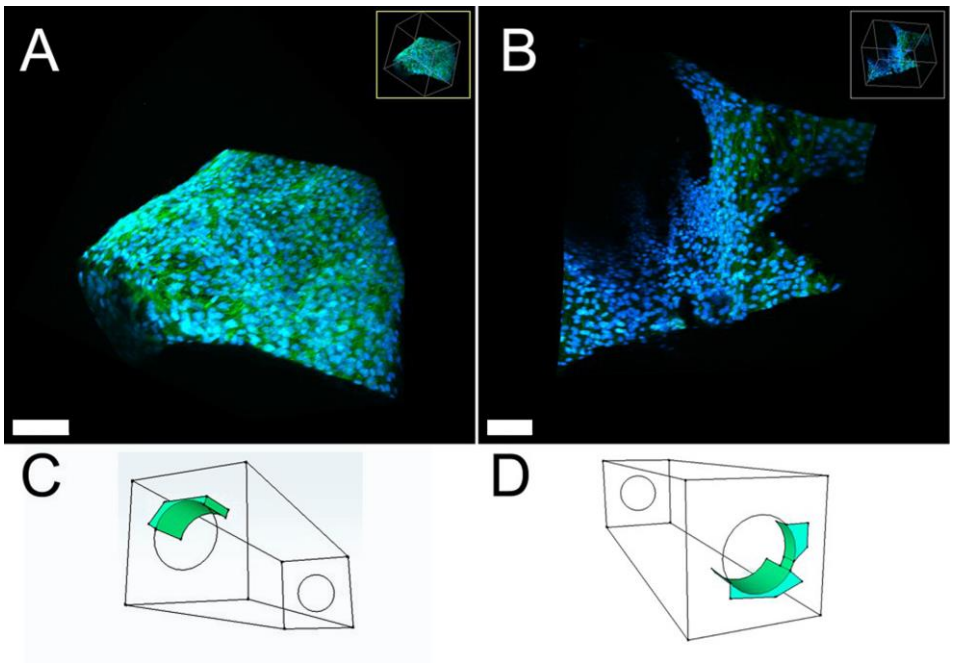

Figure S1. Multiphoton microscopy 3D reconstructions of SCs stained with DAPI and phallacidin at the end of the lumen of a HA5 **(A)** or a HA5-PLLA conduit **(B)** and schemes of the conduits with the areas where A and B were taken highlighted **(C** and **D**, respectively**)**. Scale bar = 100 μm.

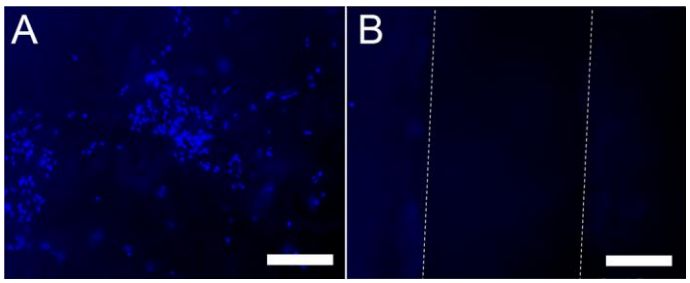

Figure S2. Fluorescence microscopy images of SCs cultured for 5 days on the outer surface of a HA5 conduit **(A)**, stained with DAPI (blue). Longitudinal cut of the same conduit with the central channel marked with dashed lines, revealing that no SC made its way through the HA5 porous wall **(B)**. Scale bar = 100 μm.